RSC Advances

PAPER

View Article Online
View Journal | View Issue

Cite this: *RSC Adv.*, 2022, **12**, 29653

The role of curing temperature and reactive aluminum species on characteristics of phosphate geopolymer

J. N. Y. Djobo, *[ab] Moustapha,[a] L. P. T. Ndjonnou,[a] K. K. Etame[a] and D. Stephan[b]

The reaction of an acid phosphate with ferro/aluminosilicate materials is a slow-setting process at room temperature that requires several days to harden. Thus, various setting accelerators are generally used to achieve quick setting and demolding in a short period. This work aims to evaluate the benefits of phosphoric acid-containing soluble aluminum and heat curing on accelerating the reaction kinetic and strength development of phosphate geopolymers. The diluted phosphoric acid (PA, 50 wt%) and acid aluminum phosphate (PA, 50 wt%, Al/P = 1/3) solutions were prepared to activate volcanic ash, and the samples were cured at 20, 40, and 60 °C to produce the phosphate geopolymer binder. The phosphate geopolymer's reaction kinetics, mechanical properties, mineralogy, and microstructure were evaluated. The results revealed that when volcanic ash was activated with diluted phosphoric acid, the reaction mechanism that prevailed was the dissolution–enhancement–precipitation–condensation, and was also fostered when the heat curing was applied. While for the acid aluminum phosphate-activated volcanic ash, the mechanism is dissolution–inhibition–precipitation–condensation. That difference in reaction mechanism led to a higher compressive strength improvement at an early age (1 d, 3 d) for room temperature cured acid aluminum phosphate activated volcanic ash. In contrast, phosphoric acid-activated volcanic ash phosphate geopolymer developed a higher compressive strength at a late age (28 d). Moreover, heat curing is the most crucial parameter having a beneficial effect on compressive strength development as compared to acid aluminum phosphate activating solution.

Received 22nd July 2022
Accepted 10th October 2022

DOI: 10.1039/d2ra04562a

rsc.li/rsc-advances

1. Introduction

The phosphate geopolymer binders have been drawing much attention in the recent decade since they stand out as great potential for broadening the fields of application of phosphate cement. The latter is made through an acid–base reaction of metal oxide (base) with an acid phosphate. It has been so far limited to a few applications because of its higher price than ordinary portland cement, the intensive heat released during the hydration process (acid–base reaction), and the poor water resistance when immersed for a longer time.[1–4] Moreover, the reactive metal oxide for phosphate cement is obtained after calcination at elevated temperature (>1300 °C) of their corresponding carbonates ($CaCO_3$, $MgCO_3$, *etc.*).[5,6] In contrast, phosphate geopolymer uses an aluminosilicate instead as a solid precursor, which is widely available and can be used as received (volcanic ash, fly ash, slag, *etc.*) or calcinated at a temperature <800 °C (clay and lateritic soils).[7–12] When compared to alkali based geopolymer, the acid phosphate activated aluminosilicate has many advantages. These involve a good resistance to corrosion and thermal resistance at elevated temperatures.[12,13] Moreover, since the reaction mechanism involve $[PO_4]$ tetrahedra with $[AlO_4]$ tetrahedral, the positive charge of the former balance the negative charge of the latter, leading to a neutral system with no efflorescence.[14,15]

The works on phosphate geopolymer have demonstrated that their properties depend on many parameters, including the chemical composition and mineralogy of the aluminosilicate (which determines their reactivity), the type and concentration of the acid phosphate solution, and the curing condition.[14,15] When calcined clay (metakaolin) is used as aluminosilicate, research works demonstrated that the reaction kinetic is slow because of the moderate dissolution rate of aluminum at room temperature, which can take several days to reach the necessary amount required to initiate the precipitation process.[16–18] So, a long initial setting time is recorded at room temperature along with weak strength development at an early age (1 to 7 days). While the use of volcanic ash containing enough reactive calcium and magnesium has been found to have a quick initial setting time and good early age (7 d) compressive strength development.[19] That was because of their rapid dissolution and the greater affinity of calcium and magnesium with phosphate

[a]*Local Material Promotion Authority (MIPROMALO), MINRESI, 2396, Nkolbikok, Yaoundé, Cameroon. E-mail: noel.djobo@mipromalo.cm/; noeldjobo@gmail.com; Fax: +237 676597699; Tel: +237 676597699*

[b]*Building Materials and Construction Chemistry, Technische Universität Berlin, Gustav-Meyer-Allee 25, 13355, Berlin, Germany*

species to form both calcium and magnesium phosphate compounds.

Regarding the type of acid phosphate solution, it was reported that the activation of high calcium fly ash with potassium dihydrogen phosphate (KH_2PO_4) gives lower strength development as compared to its counterpart obtained with diluted orthophosphoric acid (H_3PO_4) having equivalent salt content (amount of phosphate anions).[20] That is related to the particle size of KH_2PO_4 salt and its lower solubility during the acid–base reaction with fly ash, limiting the number of phosphate ions released into the system. One way to accelerate the rate of aluminum released during the reaction of aluminosilicate with acid phosphate is to apply heat curing at the initial stage of reaction, generally between 1 to 7 d.[21–23] In this regard, up to 8% of aluminum is released from metakaolin after 2 h of curing at 60 °C *versus* 3% for room temperature curing.[24] This leads to high early age compressive strength development for heat-cured metakaolin phosphate geopolymer compared with the one of geopolymer cured at room temperature, which doesn't show any strength even after 7 d. A recently published work also demonstrated that pre-curing the metakaolin phosphate geopolymer at 40 °C for 24 h followed by second curing at 60 °C and 80 °C helps to accelerate the release of aluminum, shorten the initial setting time and significantly raised the 48 h compressive strength to 120 MPa.[25] However, the effect of curing temperature on the 28 d compressive strength of iron-rich aluminosilicate (laterite) is detrimental as work reported that it (strength) decreases with the increase of the curing temperature from room temperature to 90 °C due to thermal cracking.[10] An alternative to heat curing is to use aluminum-containing acid phosphate to activate the metakaolin. Works highlighted that using soluble aluminum species with orthophosphoric acid was beneficial for enhancing the early age compressive strength and, to some extent, the late compressive strength (28 d).[26,27]

This work reports a comparative investigation of the potential benefits of the curing temperature and/or the addition of soluble aluminum species to accelerate the reaction rate and strength development of phosphoric acid-based geopolymer. On the one hand, volcanic ash was activated with dilute phosphoric acid and cured at different temperatures, while on the other hand, an acid aluminum phosphate solution was prepared and used to synthesize phosphate geopolymer at room temperature. Then, the combined effect of heat curing and acid aluminum phosphate on compressive strength development from an early age (1 d) to late age (28 d) was also assessed.

2. Experimental methods

2.1. Materials

The volcanic ash (VA) was collected in Ngaoundere, Cameroon, and ground with a planetary ball mill to reduce the particle size. The mean diameter of milled volcanic ash determined on Mastersizer 2000 of Malvern Instruments is 16.8 μm. The chemical composition of volcanic ash carried out on by X-ray fluorescence (using PW 2400, PHILIPS instruments) is: SiO_2 (42 wt%), Al_2O_3 (16 wt%), Fe_2O_3 (13.51 wt%), CaO (9.30 wt%), MgO (8.20 wt%), TiO_2 (3.02 wt%), Na_2O (2.42 wt%), MnO (0.21 wt%), K_2O (1.34 wt%), P_2O_5 (0.89 wt%) and Loss on Ignition of (2.61 wt%).

Analytical grade orthophosphoric acid, 85 wt% obtained from VWR International GmbH, Germany, was used to prepare the acid aluminum phosphate solution using the method reported in previous work.[26] The acid aluminum phosphate solution was prepared from a diluted phosphoric acid solution of 50 wt% with analytical grade aluminum hydroxide to give a final composition molar ratio Al/P = 1/3.

2.2. Synthesis of phosphate geopolymer

Two types of solutions were used for this work. These include diluted phosphoric acid (PA) of concentration 50 wt% and acid aluminum phosphate solution (MAP) having a molar ratio Al/P = 1/3 with an initial phosphoric acid concentration of 50 wt%. This composition of acid phosphate was chosen according to previous works that showed its suitability for the activation of aluminosilicate.[26,28] The paste was prepared by mixing for 3 min volcanic ash and the respective solution in a mass ratio liquid to solid of 0.45 using a KitchenAid. The details of the mix design are summarised in Table 1. The mixture was poured into 20 mm cubic molds and vibrated for 2 min. Some samples were cured at 20 °C; others were first left at 20 °C for 1 hour before curing at 40 and 60 °C for 24 h. This curing regime is used to limit thermal shock within the samples. After this initial curing, all samples were stored in a climatic room at 20 °C with 60% relative humidity until respective tests were carried out.

Table 1 Mix composition for preparing phosphate geopolymer

		Type of acid phosphate solution			
Curing temperature	Samples ID	PA	MAP	PA/powder	MAP/powder
20 °C	VAPA20	50 wt%		0.45	
	VAMAP20		50 wt% (PA) + Al/P = 1/3		0.45
40 °C	VAPA40	50 wt%		0.45	
	VAMAP40		50 wt% (PA) + Al/P = 1/3		0.45
60 °C	VAPA60	50 wt%		0.45	
	VAMAP60		50 wt% (PA) + Al/P = 1/3		0.45

2.3. Characterization methods

The isothermal calorimetry was carried out on TAM Air 3 calorimeter (TA Instruments) operating at 20 °C for 24 h. For this test, 5 g of VA were mixed with the corresponding activating solution (liquid to solid mass ratio of 0.45) outside the calorimeter. The time elapsed between mixing and loading the sample into the calorimeter was 1 min. Because of external mixing, we could not perform the analysis at 40 and 60 °C. Since the heat change while inserting the outside mixed sample into the calorimeter rather gives rise to an endothermic peak.

The compressive strength evolution was measured 20 mm cubic molds after 1, 3, 7, and 28 d using a compression testing machine (Toni Technik, Berlin, Germany). The results are the average value of 3 tested samples for each formulation.

The mineralogical and molecular characterization of volcanic ash and hardened geopolymers were determined using X-ray diffractometry (XRD) and Fourier transformed Infrared Spectroscopy (FTIR), respectively. XRD was performed on an Empyrean PANalytical diffractometer with Ni filter CuKα radiation ($\lambda k_{\alpha_1} = 1.540598$ Å) at the slow scan from 5 to 65° 2θ. High Score Plus software was used to identify different crystalline phases. Further quantitative phase analysis using Rietveld refinement was performed *via* internal standard (10 wt% rutile). The refinement was done with HighScore Plus 4.8 (PANalytical) using the crystallographic structure files of the ICSD (Inorganic Crystal Structure Database). FTIR spectra by the attenuated total reflectance method were recorded using PerkinElmer instruments operating in the wavelength range 400 to 4000 cm^{-1} with a resolution of 1 cm^{-1}.

The thermal gravimetry analysis (TGA) coupled with differential scanning calorimetry of the crushed samples of the hardened phosphate geopolymer from the compressive test was performed on Mettler Toledo 3 + SARe System (Mettler Toledo, USA). The temperature varies from 25 °C to 1000 °C at a heating rate of 5 °C min^{-1} under a controlled atmosphere with synthetic air flowing at 70 mL min^{-1}.

The mercury intrusion porosimetry (Pascal series 140/240, from ThermoScientific) was used to determine the pore size distribution of the fractured samples. The microstructure was determined using a scanning electron microscope (SEM) with a backscatter detector and coupled with energy-dispersive X-ray spectroscopy (EDX) (Zeiss Gemini SEM 500 NanoVP microscope Oberkochen, Germany). The device operated in low-vacuum mode with 15 kV acceleration voltage.

3. Results and discussion

3.1. Reaction kinetic

The heat evolution during the reaction of volcanic ash with phosphoric acid and acid aluminum phosphate solution at 20 °C is depicted in Fig. 1. The heat flow evolution is characterized by an exothermic peak whose maximum is reached in a few minutes (5 min), then decreases and becomes constant with time. While the total heat released, first increases significantly with time before reaching a plateau where the rate of heat released decreases. The exothermic peak corresponds to the dissolution of reactive components in volcanic ash by an acid–base reaction, followed by their precipitation–condensation to a gel of different phases.[19] The total heat released by the volcanic ash activated with phosphoric acid is higher than the one activated with acid aluminum phosphate. This indicates that phosphoric acid speeds up the dissolution process of volcanic ash more than acid aluminum phosphate. That is due to the degree of acidity of the different solutions since the acid aluminum phosphate has a higher pH (0.8) as compared to a phosphoric acid solution with the same phosphate content (<0.5).[26] Thus, knowing that the dissolution of the main soluble elements (Fe and Al) present in volcanic ash increases when the pH of the acid solution decreases,[19,29] this explains the difference in heat released by the two kinds of acid phosphate solution.

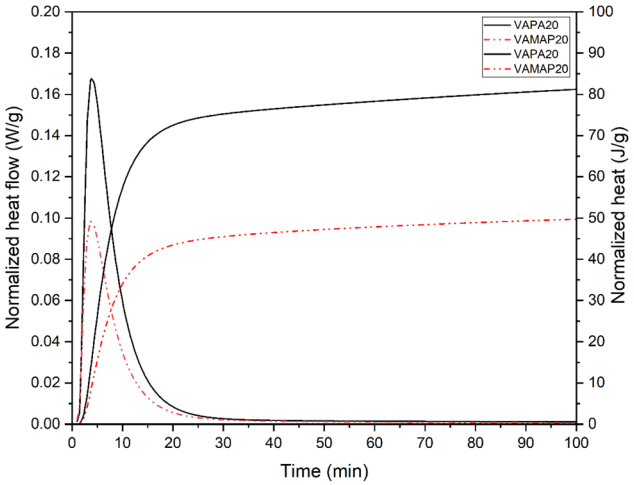

Fig. 1 Isothermal calorimetry of phosphate geopolymer at 20 °C (plain line = VAPA, dotted line = VAMAP).

3.2. Relationship between reaction progress and strength development

The influence of curing temperature and type of acid phosphate solution on the structural development of volcanic ash phosphate geopolymer is shown in Fig. 2. In general, compressive strength evolves with time, and applying heat curing helps accelerate compressive strength development at an early age. One can see that phosphoric acid-activated volcanic ash did not show any strength at 1 d when cured at 20 °C, whereas curing at 40 and 60 °C helped achieve 11 MPa and 20 MPa, respectively, at the same date (1 d). That observation demonstrates the benefit of temperature in accelerating the rate of aluminum released from volcanic ash. That is because the dissolution rate of aluminum in phosphoric acid is very slow, and previous work reported that using heat curing speeds up that reaction.[30] It is known from the literature that aluminum and iron from volcanic ash are responsible for strength development, while calcium and magnesium ensure a fast setting at room temperature.[19] Knowing that the dissolution rate of iron in phosphoric acid at room temperature is faster, one can surmise that such a good strength development while curing is related to the

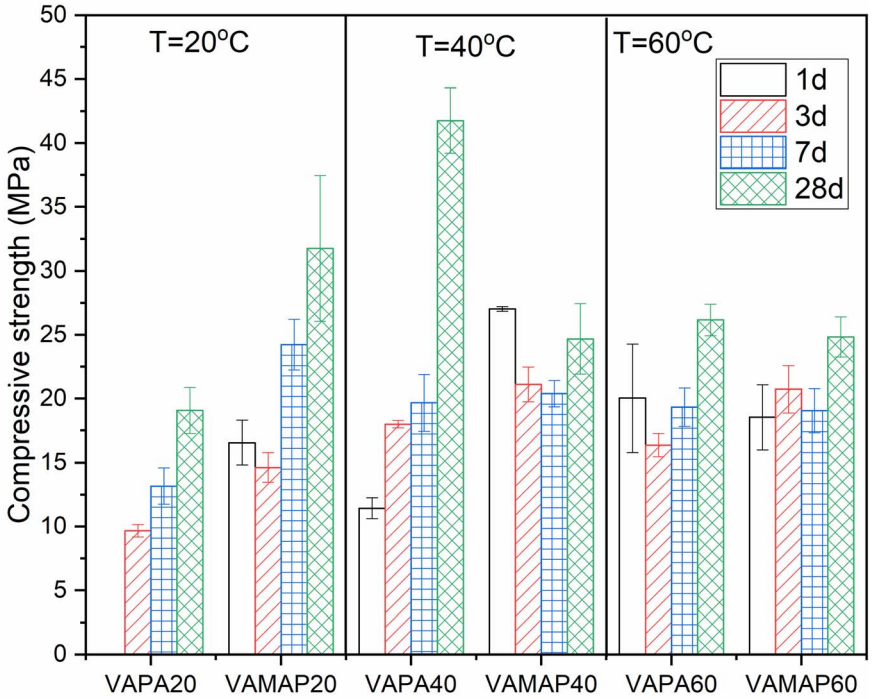

Fig. 2 Compressive strength evolution of volcanic ash phosphate geopolymer.

availability of aluminum. This rapidly triggers the second step of the reaction, which is precipitation condensation leading to the gels that develop structural characteristics.

The abovementioned observations can be supported by the strength development of acid aluminum phosphate-activated volcanic ash. The binder developed a 1 d compressive strength of 16.6, 27, and 18.5 MPa at 20, 40, and 60 °C, respectively. Compared with phosphoric acid-activated volcanic ash, it is obvious that the availability of soluble aluminum in the acid solution has fostered the rate of formation of the gels constituting the binder at room temperature. Besides, when applying high curing temperature, the 28 d compressive strength of the acid aluminum phosphate activated volcanic ash samples decreases considerably as compared to the one cured at room temperature. But it does not change significantly when the curing temperature increases to 40 °C (24.68 MPa) and 60 °C (24.85 MPa). While the 28 d compressive strength of the phosphoric acid-activated volcanic ash (VAPA) reaches 42 MPa after curing temperature at 40 °C. Then, it decreases significantly to 26 MPa at 60 °C. A similar trend was observed on the acid–phosphate activation of lateritic soils with a compressive strength decrease from 83 MPa at room temperature to 24 MPa at 90 °C.[10] Another work reported slight changes in the 28 d compressive strength of phosphoric acid-activated volcanic ash when cured at 28 °C (34 MPa) and 60 °C (37 MPa).[31] Therefore, though the curing temperature is interesting for accelerating the reaction rate, the rapid formation of the gels at an early age inhibits further reaction progress with time, which also limits the compressive strength increases at a late age.[32] This is also true for the acid aluminum phosphate activated volcanic ash, where the speeding up of the precipitation condensation reaction in the formation of the gels makes useless additional heat treatment for the strength development.

3.3. Mineralogical characteristics

Fig. 3 depicts the XRD patterns of phosphate geopolymers. The minerals observed are Magnetite (Fe_3O_4, PDF 98-009-8084), Hematite (Fe_2O_3, PDF 98-001-5840), Forsterite ferroan ($Fe_{0.278}Mg_{1.722}SiO_4$, PDF 98-007-9171), Anorthite ($CaAl_2Si_2O_8$, PDF 98-008-6319), and Augite ($CaFe_{0.25}Mg_{0.74}Si_2O_6$, PDF 98-009-0143). Those minerals are the same that were initially present in volcanic ash. However, there is a change in their intensity and the height of the broader hump between 20 and 37° 2 theta. That hump is characteristic of the content of reacted phase in an amorphous state. The quantitative phase analysis was performed using the Rietveld method to highlight the changes better, and the results are reported in Table 2.

Volcanic ash comprises 48.9 wt% of augite, 28 wt% of anorthite, 5.6 wt% forsterite, ferroan, 2.6 wt% magnetite, 0.5 wt% hematite, and 14.4 wt% of an amorphous phase. In the phosphate geopolymer activated with phosphoric acid, the amorphous content increases to 18.9 wt%, 33,1 wt%, and 32.4 wt% with rising curing temperatures of 20, 40, and 60 °C, respectively. While for the acid aluminum phosphate activated volcanic ash, it is 44.6 wt%, 53.5 wt%, and 50.5 wt% with increasing curing temperatures of 20, 40, and 60 °C, respectively. The change in the amorphous content for phosphate geopolymer activated with phosphoric acid correlates well with the change in compressive strength, as the sample cured at

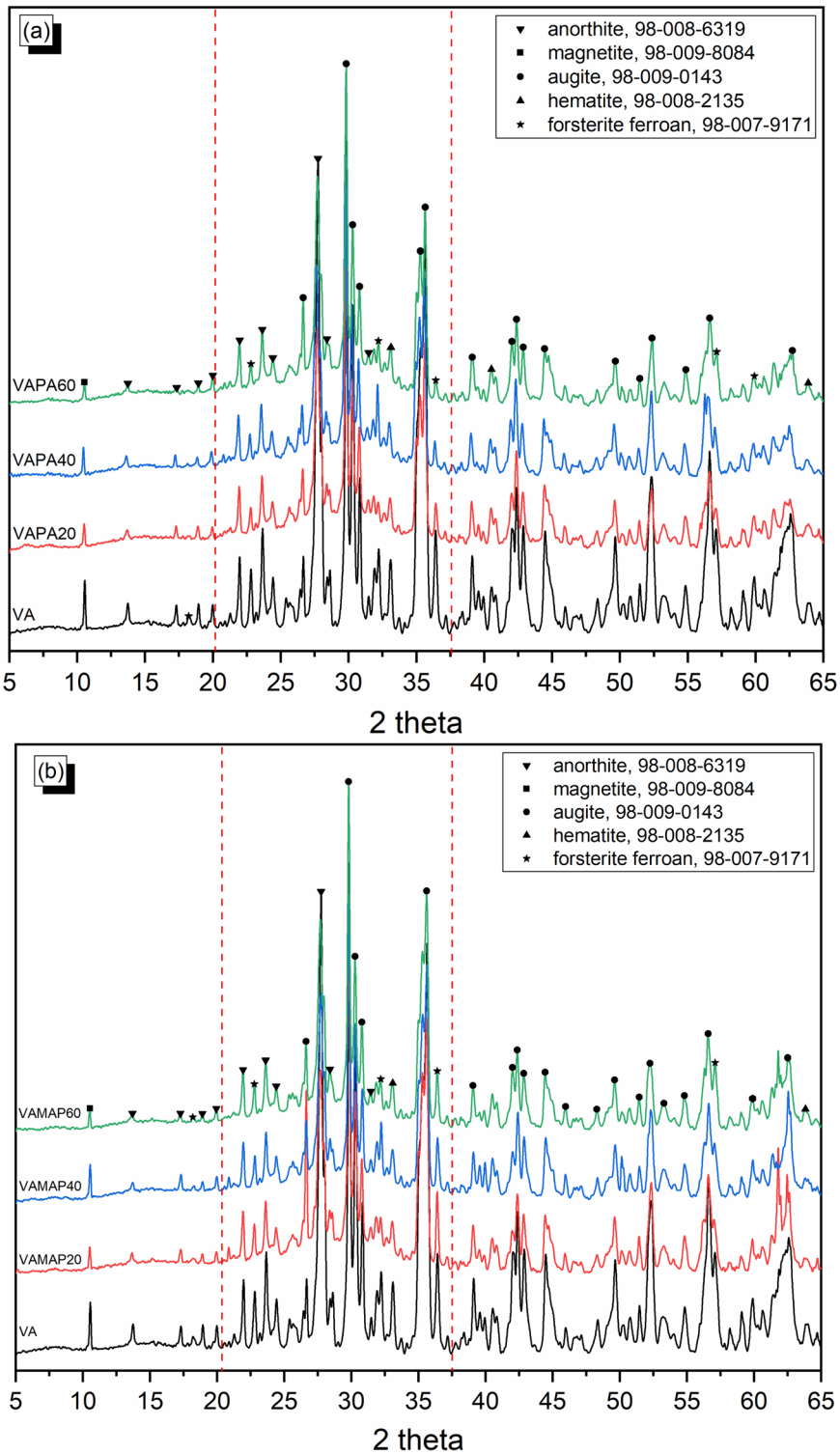

Fig. 3 XRD patterns of volcanic ash phosphate geopolymer: (a) obtained with diluted phosphoric acid, (b) obtained with monoaluminum phosphate (MAP).

40 °C has the higher amount of reacted phases corresponding to the highest strength development. Nevertheless, the content of reacted phase of acid aluminum phosphate activated geopolymer binder is higher than the one obtained with diluted phosphoric acid, which does not correlate with the compressive strength development at 28 d. That could be related to the drying of the remaining aluminum phosphate present in the acid aluminum phosphate solution that did not take part in the reaction. It is worth noting that the acid aluminum phosphate solution when dried at a temperature <100 °C, is amorphous.[36]

Table 2 Quantitative phase analysis of volcanic ash and phosphate geopolymers using the Rietveld method

	Minerals phases content (wt%)					
Samples ID	Augite	Anorthite	Forsterite, ferroan	Magnetite	Hematite	Amorphous
VA	48.9	28.0	5.6	2.6	0.5	14.4
VAPA20	46.4	30.9	1.4	1.5	0.8	18.9
VAPA40	33.0	30.7	1.4	0.9	0.9	33.1
VAPA60	34.8	28.9	2.2	0.7	0.9	32.4
VAMAP20	28.6	21.1	3.1	1.8	0.8	44.6
VAMAP40	24.5	17.0	3.0	1.4	0.6	53.5
VAMAP60	25.1	19.0	3.3	1.5	0.7	50.5

So it is likely that it would have contributed to the increase of the amorphous content without any effect on the compressive strength improvement. Since the compressive strength of this acid aluminum phosphate series decreases with the rising curing temperature (Fig. 2).

The influence of heat curing and the soluble aluminum on the molecular structure of the reacted products are assessed by infrared spectrometry are shown in Fig. 4. IR spectra of the phosphate geopolymer were presented in the region 600–2000 cm^{-1}, where the most significant changes can be observed. The main band centered at 998 cm^{-1} is characteristic of the stretching vibration of Si–O–T, where T corresponds to Si, Al, and Fe of the aluminosilicate network in volcanic ash.[19] In the phosphate geopolymer, the main band appears at higher wavenumber 1060–1070 cm^{-1} and 1040–1058 cm^{-1}, respectively, for phosphoric acid and acid aluminum phosphate activated volcanic ash. That main band is characteristic of the stretching vibration of the P–O–(Fe), P–O–(Al) and P–O–(Si) bonds of the reaction products (binder).[35] That band is accompanied by the one appearing as a small shoulder at 910 cm^{-1}, also characteristic of vibration of P–O of the phosphate binder. The band at 1640 cm^{-1} is characteristic of the bending vibration of H–O bonds of water. The difference in the wavenumber of the main band indicates that the bond constituting the reacted products of phosphoric acid-activated volcanic ash is stronger than in the acid aluminum phosphate-activated volcanic ash. That is because a higher wavenumber means higher energy requires to trigger the vibration of that bond.[26] This observation agrees with previous results from this paper which demonstrated that a higher extent of dissolution–precipitation along with condensation was achieved in phosphoric acid-activated volcanic ash compared to acid aluminum phosphate-activated volcanic ash binder.

Fig. 5 shows the mass loss and phase changes of the phosphate binder. A major mass loss starts at nearly room temperature to ends at 600 °C and is accompanied by an endothermic peak centered at 90–98 °C in the DSC curves. It is characteristic of the loose of both physically and chemically bound water in the phosphate binder. Between 600 and 700 °C, two exothermic peaks are identified with no noticeable mass change. In phosphoric acid-activated volcanic ash (Fig. 5a), the two peaks are well resolved and centered at 635 and 697 °C. For acid aluminum phosphate activated volcanic ash (Fig. 5b), the peaks are centered at 640 and 686 °C. The peak at 635–640 °C corresponds to the partial crystallization of the amorphous phase constituting the binder in ferrous/ferric phosphate minerals.[12] The peak at 686–697 °C is related to the partial crystallization of the amorphous phase of the phosphate binder in aluminum phosphate minerals.[35,37] These two peaks are well visible in the DSC curves of all phosphoric acid-activated volcanic ash, while it is only visible on the curve of acid aluminum phosphate geopolymer cured at room temperature. That observation can be attributed to the extent of the reaction and the amount of reacted products formed. This means that a high amount of reacted product was formed when phosphoric acid was used as an activator compared to volcanic ash activated with acid aluminum phosphate binder. In addition, it also indicates that a higher content of reacted phase has been formed in room temperature cured acid aluminum phosphate activated volcanic ash binder. All of these agree with the mechanical test results, where the highest 28 d compressive strength was developed by phosphoric acid activated volcanic ash binder. While for acid aluminum phosphate activated volcanic ash binder, a higher 28 d compressive strength was obtained when room temperature curing was applied.

3.4. Microstructural characteristics

The pore size distribution and the relative pore volume distribution of the different phosphate geopolymers are shown in Fig. 6 and 7, respectively. As seen in Fig. 6, the size of the pores ranges from 0.01 μm to 100 μm, corresponding to capillary pores and air pores.[21] However, the relative pore volume distribution gives more information on the nature of the porosity. From Fig. 7, the maximum of pores ranges from 0.01 μm to 10 μm, which indicates that capillary pores are dominant in the phosphate geopolymer prepared. In addition, all the samples show several peaks maximum, which corresponds to a multimodal pore volume distribution. The fact that these peaks are linked indicates that those pores are connected, which confirms the predominance of capillary pores in the present system. The calculation of the mean pore diameter(d_m) as the average of the characteristic diameters (d_{90}, d_{50}, and d_{10}) helps to better visualize and compare the size of the pores in each system. The d_m is 5.98 μm, 4.54 μm, and 8.54 μm for VAPA20, VAPA40, and VAPA60, respectively. For the VAMAP

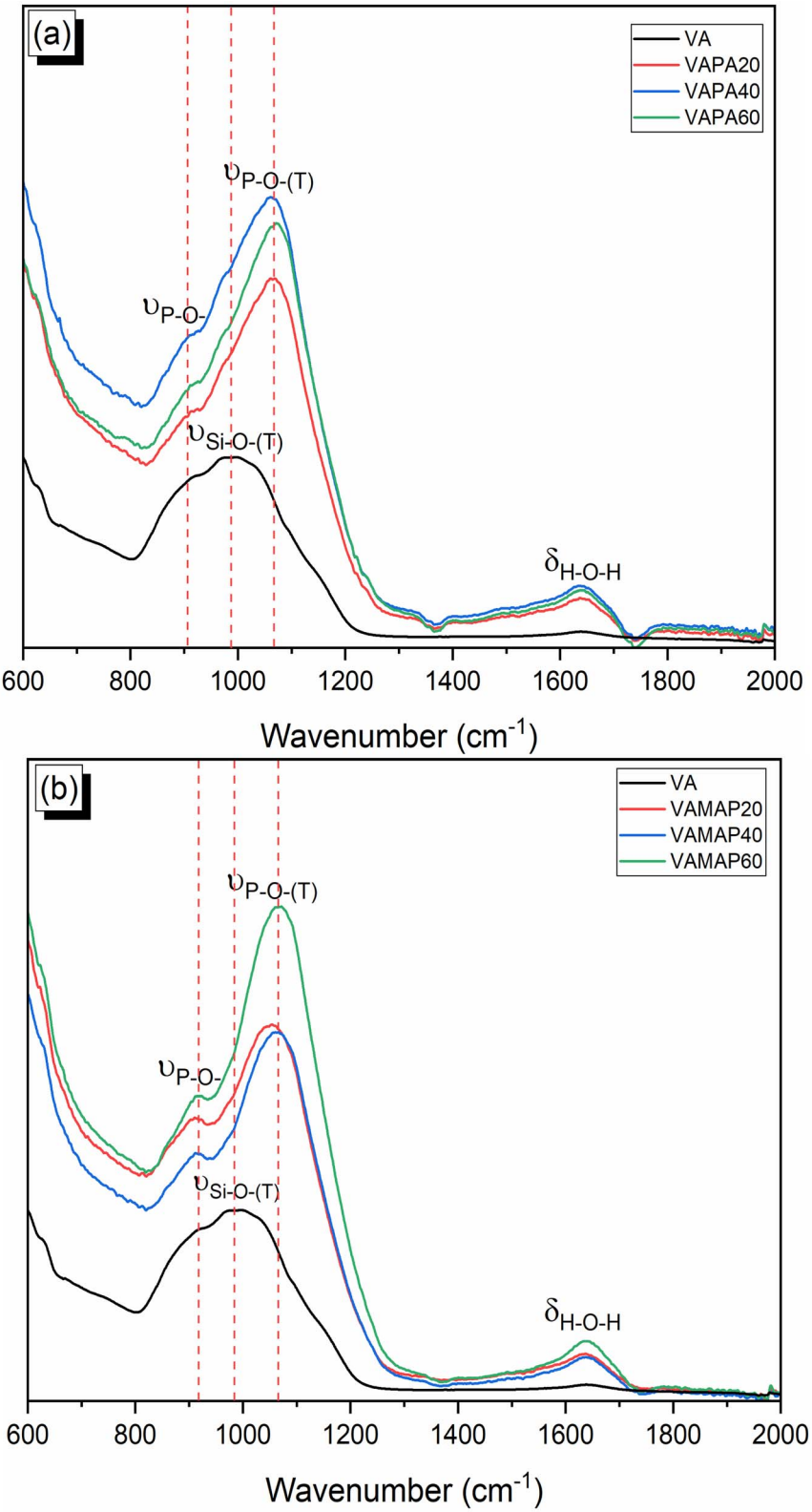

Fig. 4 FTIR spectra of volcanic ash phosphate geopolymer: (a) obtained with diluted phosphoric acid, (b) obtained with monoaluminum phosphate (MAP).

series, d_m is 0.996 μm, 0.704 μm, and 2.046 μm with the increase of curing temperatures of 20, 40, and 60 °C, respectively. These results show that the phosphoric acid-activated volcanic ash-based geopolymer binders (VAPA) have a higher pore size than the acid aluminum phosphate-activated volcanic ash-based geopolymer binders (VAMAP). However, the distribution

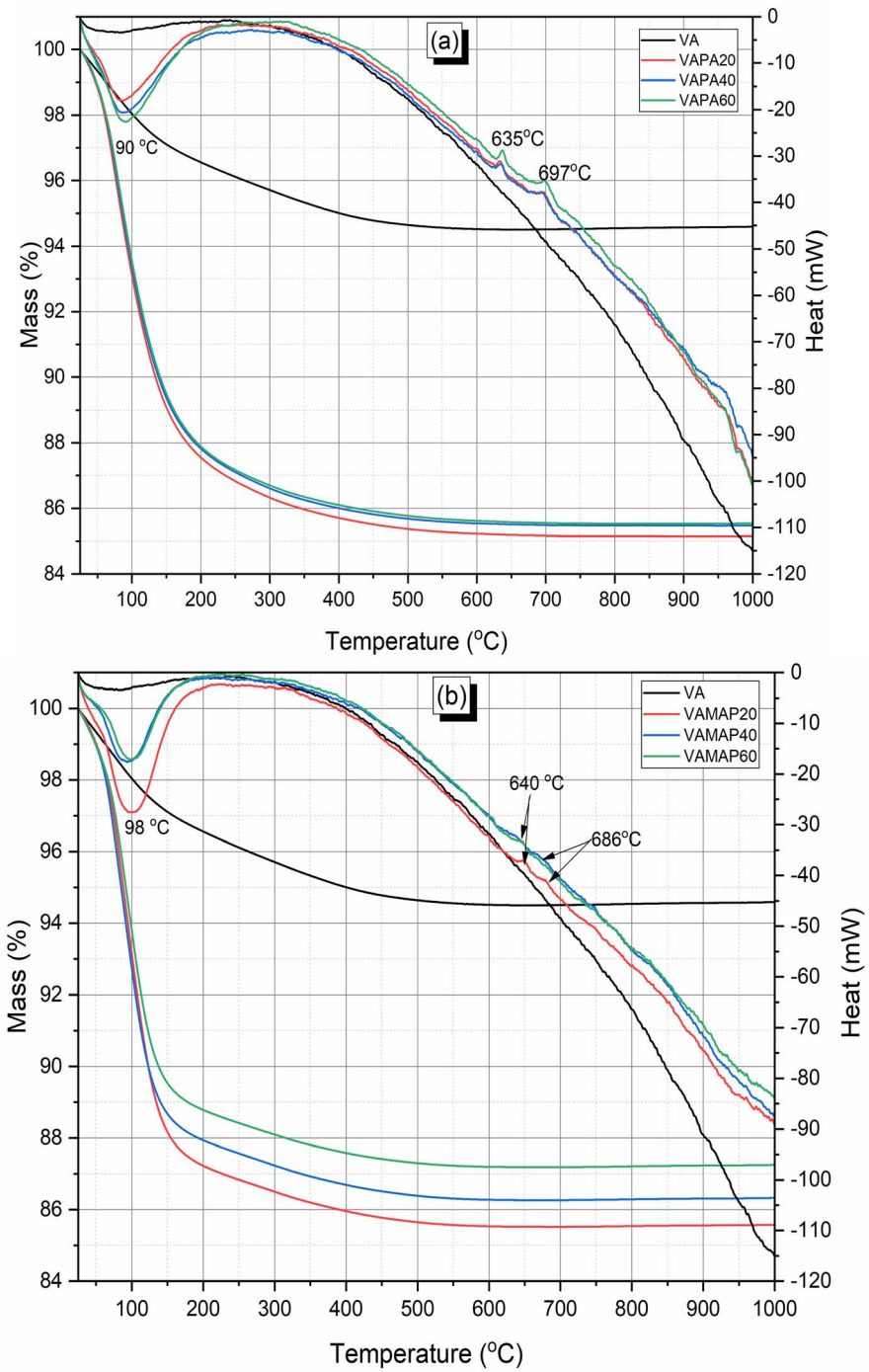

Fig. 5 TGA-DSC of volcanic ash phosphate geopolymer: (a) obtained with diluted phosphoric acid, (b) obtained with monoaluminum phosphate (MAP).

of the relative pore volume (Fig. 7) shows that the VAMAP series have high pore volume in the pore size range of 0.01 μm to 10 μm than the VAPA series. This demonstrates that though the acid aluminum phosphate-activated volcanic ash-based geopolymer binders (Fig. 7b) have the smallest pore diameter, their amount remains higher than the total pore of phosphoric acid-activated volcanic ash-based geopolymer binders (Fig. 7a). Therefore, the VAPA series has a lower porosity than the VAMAP series. Finally, these results stressed that a faster reaction kinetic limits the extent of the reaction and the formation of a high-volume binder (reacted products) which increases the porosity of the matrix.

The phase assembly and texture of the phosphate geopolymer obtained from scanning electron microscopy are depicted in Fig. 8. The micrographs of all samples are heterogenous in their textures with the presence of multiple cracks and pores. The presence of multiple cracks can be due to the release during the drying of the remaining water that did not

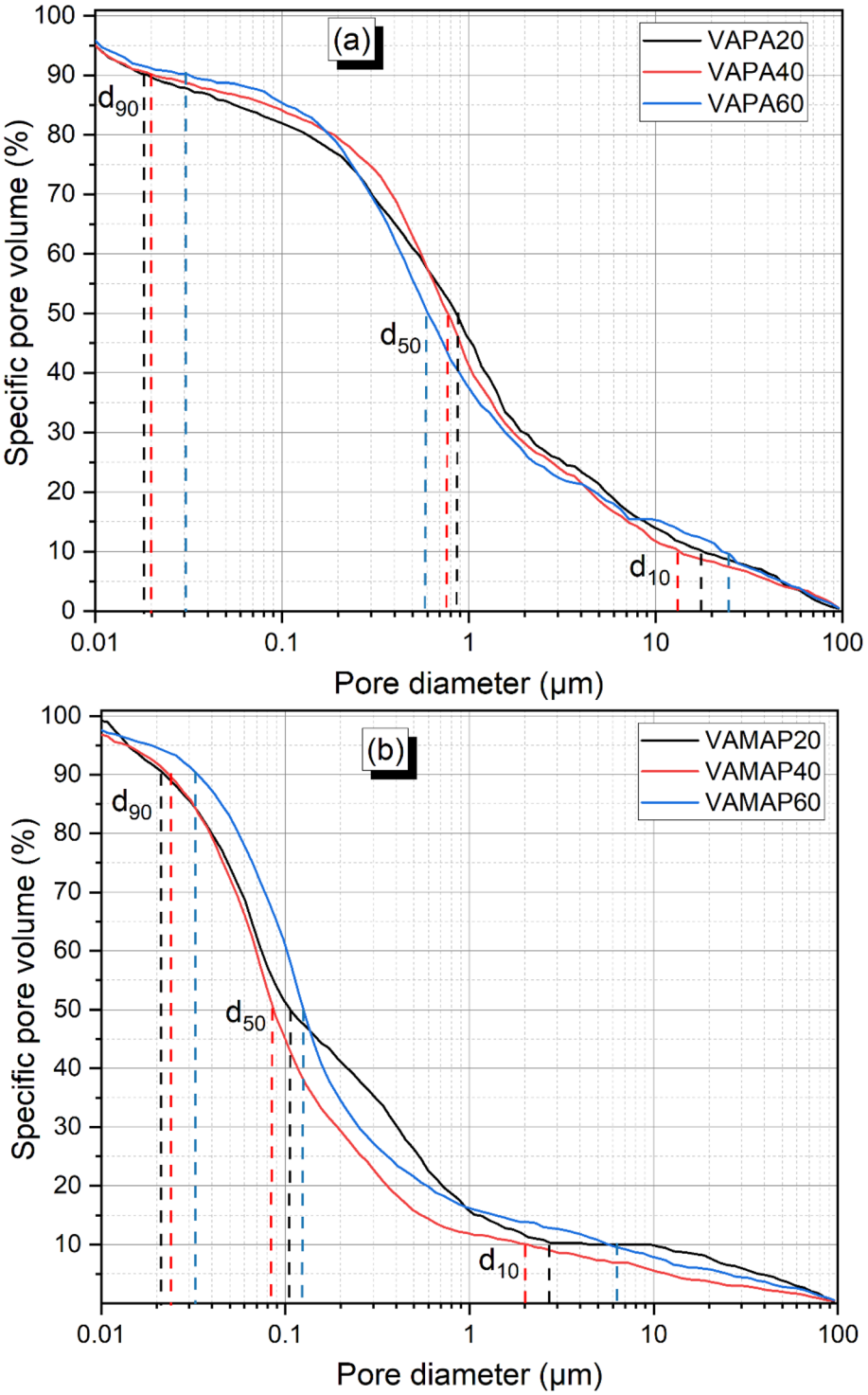

Fig. 6 Pore size distribution of (a) phosphoric acid activated volcanic ash-based geopolymer binder with varying curing temperatures acid, (b) acid aluminum phosphate activated volcanic ash-based geopolymer binder with varying curing temperatures.

take part in the reaction. The phases observed are shapeless and the EDX point analysis on at least forty points in each sample was carried out to differentiate the phases present. Here the unreacted phases are considered as those having high content of Si, Al, Fe, Ca, and Mg without P or very few amount of it. Whereas the binder consists of a mixture of all the elements in an equilibrated proportion. The data collected are summarised in Table 3, where only the composition of the distinct phases available in the matrix is presented. Three main phases are identified in all samples. These involve coarse particles of volcanic ash that did not participate in the reaction. Those unreacted particles are characterized by a very high Si/P atomic

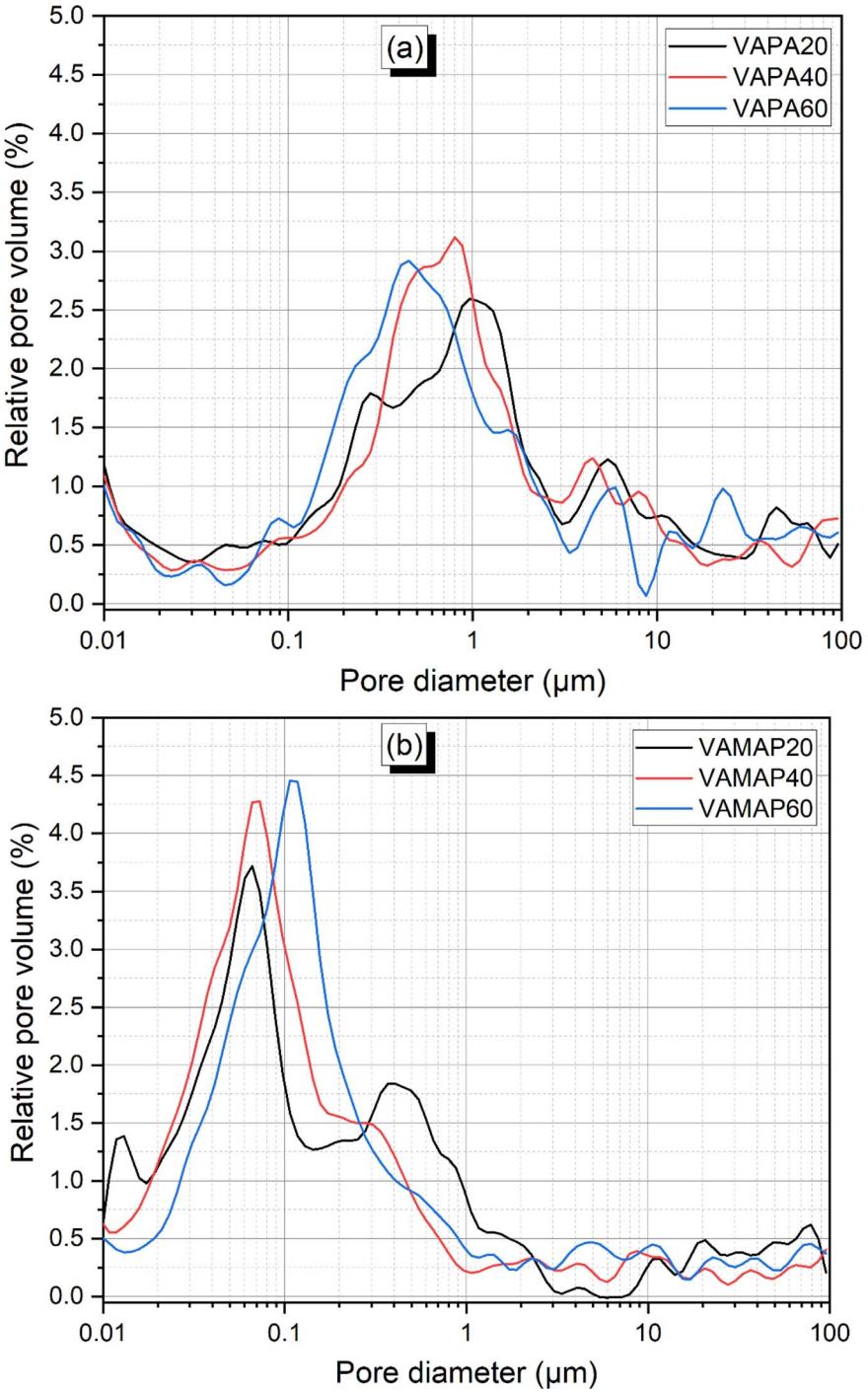

Fig. 7 Relative pore volume distribution of (a) phosphoric acid activated volcanic ash-based geopolymer binder with varying curing temperatures acid, (b) acid aluminum phosphate activated volcanic ash-based geopolymer binder with varying curing temperatures.

ratio. This also agrees with the literature that proved the limited participation of the silicon during the acid phosphate activation of an aluminosilicate.[9,19] Two main phases corresponding to the reacted products are also identified, one is silicon-rich with a formula close to $(Mg, Ca)_x(Al, Fe, Si)_y(H_2PO_4)_z$ and the other is silicon-free $(Mg, Ca)_x(Al, Fe)_y(H_2PO_4)_z$, where x, y and z are the stoichiometry of different elements. These were also observed in previous work and reported to be the main reacted product resulting from the acid phosphate activation of volcanic ash.[35] It thus confirms that though silicon solubility is weak in an acid phosphate solution, the part dissolved takes part in the reaction and modifies the chemistry of the binder. Elsewhere, the presence of soluble aluminum species in the activating solution and the curing temperature did not affect the phase formed.

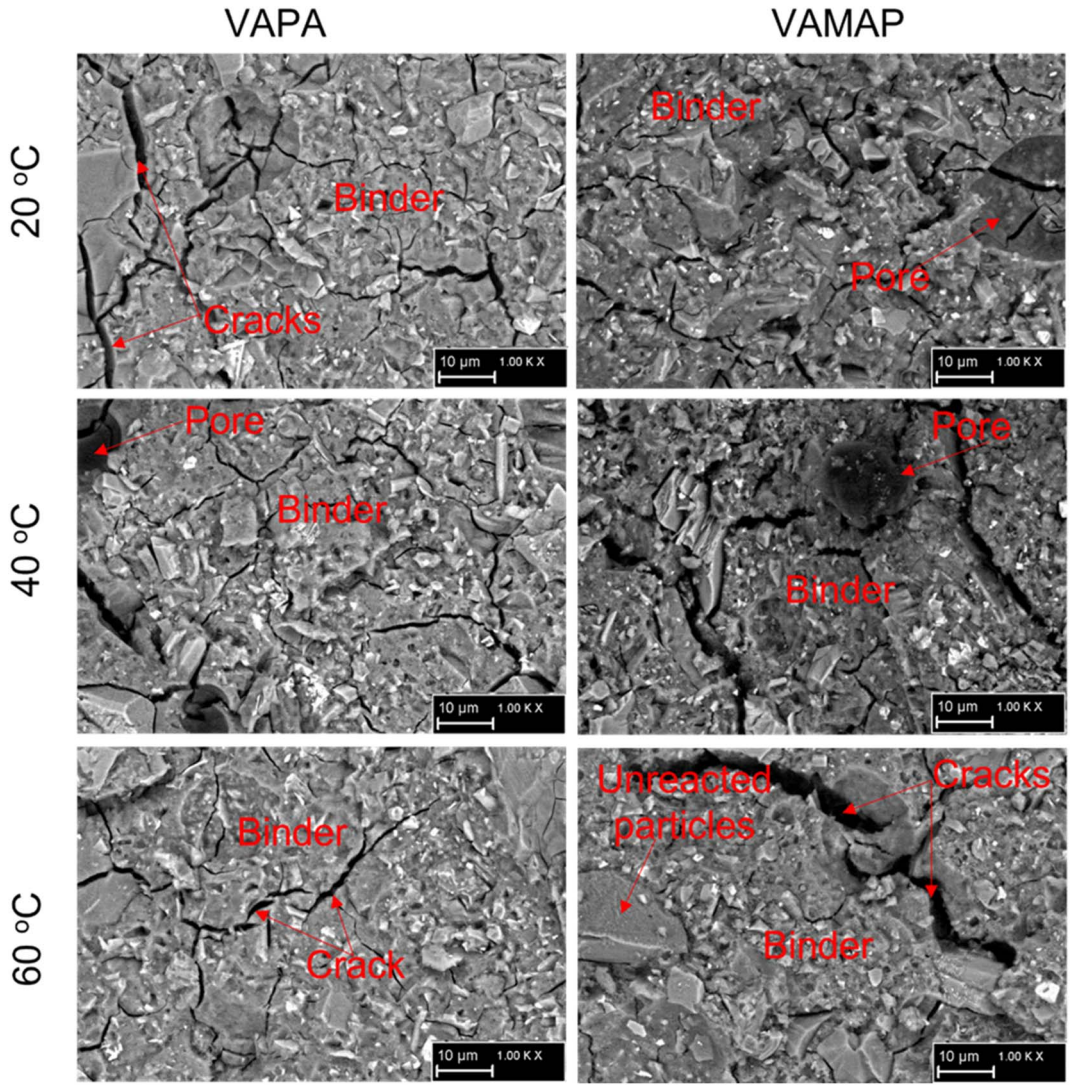

Fig. 8 Backscattered scanning electron micrograph of volcanic ash-based phosphate geopolymer binder with varying curing temperatures acid.

3.5. The reaction mechanism and the influence of different synthesis conditions

The exploitation of the reaction kinetic result, the compressive strength evolution, and the microstructural analysis presented above have given a better understanding of the reaction process ongoing. It is observed that when volcanic ash is activated with diluted phosphoric acid, there is a continuous dissolution over time along with precipitation–condensation that contributes to the formation of high-volume binder at a late age. Besides, applying heat curing up to 40 °C foster the process, while higher temperatures show the reverse benefit. This agrees with previous work which demonstrated slow dowing of the reaction progress when a phosphoric acid concentration beyond 8–10 M was used.[19,33,34] One can argue that, beyond 40 °C, the precipitation and condensation process takes over the dissolution reaction since the amount of dissolved elements is already sufficient to undergo that process. Thus it can be proposed that the reaction mechanism occurring, in this case, is the dissolution enhancement followed by the precipitation of the dissolved species when their concentrations become significant. Which allows high condensation rate and compressive strength improvement with time. When the initial phosphoric acid is modified with a soluble aluminum as a way to accelerate the setting at room temperature the precipitation–condensation process compete with the dissolution during the formation of the binder. That corroborates with previous works which demonstrated that the use of calcium-based setting accelerator (slag, calcium hydroxide, calcium silicate *etc.*) was beneficial only for improving compressive strength at an early age.[28,32] Since, the control phosphate binder without setting accelerators developed better strength at a late age. That is because the limited dissolution of the ferro/aluminosilicate was recorded due to the lowering of the acidity attributed to the acid–base reaction that occurred at the beginning of the reaction.[26,35] As a general rule, the dissolution–enhancement–precipitation–condensation is the reaction mechanism dominating the phosphoric acid activation of ferro/aluminosilicate at room or

Table 3 EDX analysis and phase composition of volcanic ash-based phosphate geopolymer

	Atomic ratio					
Samples	Al/P	Fe/P	Si/P	Ca/P	Mg/P	Phases
VAPA20	5.31	1.93	9.54	2.11	1.02	Unreacted phase
	0.65	4.96	0	0.77	1.17	$(Mg, Ca)_x(Al, Fe)_y(H_2PO_4)_z$
	1.79	2.28	1.92	1.34	1.92	$(Mg, Ca)_x(Al, Fe, Si)_y(H_2PO_4)_z$
VAPA40	2.89	4.91	9.63	13.77	4.63	Unreacted phase
	0.91	5.23	0.11	0.93	1.24	$(Mg, Ca)_x(Al, Fe)_y(H_2PO_4)_z$
	1.24	4.35	1.59	1.55	1.06	$(Mg, Ca)_x(Al, Fe, Si)_y(H_2PO_4)_z$
VAPA60	5.69	4.56	10.36	6.33	7.29	Unreacted phase
	0.94	4.41	0.64	1.28	0.65	$(Mg, Ca)_x(Al, Fe)_y(H_2PO_4)_z$
	1.83	3.17	1.62	1.00	0.65	$(Mg, Ca)_x(Al, Fe, Si)_y(H_2PO_4)_z$
VAMAP20	4.21	1.00	15.78	2.06	0.82	Unreacted phase
	2.17	2.48	0.54	0.59	0.28	$(Mg, Ca)_x(Al, Fe)_y(H_2PO_4)_z$
	2.13	2.49	1.43	1.47	1.27	$(Mg, Ca)_x(Al, Fe, Si)_y(H_2PO_4)_z$
VAMAP40	8.07	5.75	14.15	9.91	8.65	Unreacted phase
	1.5	1.85	0.17	4.45	0.14	$(Mg, Ca)_x(Al, Fe)_y(H_2PO_4)_z$
	2.61	1.55	1.41	1.02	1.21	$(Mg, Ca)_x(Al, Fe, Si)_y(H_2PO_4)_z$
VAMAP60	7.14	1.02	13.07	3.54	0.32	Unreacted phase
	2.24	2.58	0	0.33	0.08	$(Mg, Ca)_x(Al, Fe)_y(H_2PO_4)_z$
	2.67	2.13	1.74	0.93	0.89	$(Mg, Ca)_x(Al, Fe, Si)_y(H_2PO_4)_z$

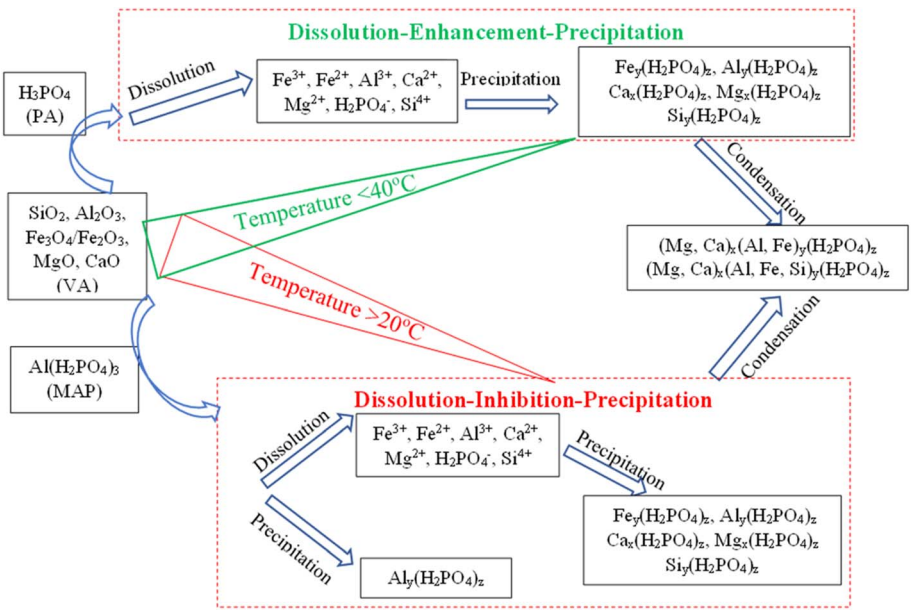

Fig. 9 Schematic diagram of the reaction mechanism of acid phosphate activation of volcanic ash at different synthesis conditions.

mild temperatures. Whereas, at high temperatures or in presence of any setting accelerators, the dissolution–inhibition–precipitation–condensation is the dominant reaction mechanism. Fig. 9 summarises the reaction mechanism occurring in the acid phosphate activation of volcanic ash.

4. Conclusion

This work has reported the benefits of an acid phosphate containing soluble aluminum, and the application of heat curing in the preparation of volcanic ash phosphate geopolymer binders. The main findings are summarised as follow:

(1) The use of acid phosphate solution containing soluble aluminum species at room temperature forsters the precipitation–condensation reaction and strength development at an early age. Whereas, albeit diluted phosphoric acid accelerated the dissolution rate of volcanic ash, the low content of aluminum species delayed the reaction kinetic and compressive strength development.

(2) The heat curing of phosphate geopolymer binder enhances the development of compressive strength at any age of phosphate geopolymer activated with diluted phosphoric

acid. The maximum improvement is obtained with a curing temperature of 40 °C.

(3) Finally, the curing temperature is the most beneficial parameter for accelerating the reaction kinetic compared to diluted phosphoric acid-containing soluble aluminum. That is because heat not only improves the dissolution of aluminum from volcanic ash but also forsters the solubility of other reactive components, including iron, calcium, magnesium, and somewhat silicon.

Conflicts of interest

There are no conflicts to declare.

Acknowledgements

The work was supported by the Alexander von Humboldt Foundation through the Georg Forster Research Fellowship for Postdoctoral Researchers (CM-1201499-GF-P) awarded to Dr Djobo. The technical assistance of Mr Tobias Dorn in carrying out the SEM-EDX analysis is appreciated.

References

1 L. Lv, P. Huang, L. Mo, M. Deng, J. Qian and A. Wang, *Constr. Build. Mater.*, 2019, **203**, 589–600.
2 Y. Liu, Z. Qin and B. Chen, *Constr. Build. Mater.*, 2020, **231**, 117131.
3 Y. Liu, B. Chen, Z. Qin, D. Pen and M. Aminul Haque, *Constr. Build. Mater.*, 2020, **257**, 119570.
4 Y. Liu, Z. Qin and B. Chen, *Constr. Build. Mater.*, 2020, **242**, 118052.
5 M. Gao, B. Chen, L. Lang and R. A. Muhammad, *J. Mater. Civ. Eng.*, 2020, **32**, 1–11.
6 Y. Li, J. Sun and B. Chen, *Constr. Build. Mater.*, 2014, **65**, 177–183.
7 H. Guo, B. Zhang, L. Deng, P. Yuan, M. Li and Q. Wang, *Appl. Clay Sci.*, 2021, **204**, 106019.
8 H. Majdoubi, Y. Haddaji, S. Mansouri, D. Alaoui, Y. Tamraoui, N. Semlal, M. Oumam, B. Manoun and H. Hannache, *Eng. Contract.*, 2021, **35**, 102078.
9 B. Zhang, H. Guo, P. Yuan, L. Deng, X. Zhong, Y. Li, Q. Wang and D. Liu, *Cem. Concr. Compos.*, 2020, **110**, 103601.
10 C. N. Bewa, H. K. Tchakouté, C. H. Rüscher, E. Kamseu and C. Leonelli, *SN Appl. Sci.*, 2019, **1**, 1–12.
11 V. Mathivet, J. Jouin, A. Gharzouni, I. Sobrados, H. Celerier, S. Rossignol and M. Parlier, *J. Non-Cryst. Solids*, 2019, **512**, 90–97.
12 J. N. Y. Djobo, A. Elimbi and D. Stephan, *SN Appl. Sci.*, 2020, **2**, 828.
13 A. S. Wagh, in *Developments in Strategie Materials and Computational Design II Developments in Strategie Materials and Computational Design II*, ed. W. M. Kriven, A. L. Gyekenyesi and J. Wang, John Wiley & Sons, Inc, Hoboken, New Jersey, 2011, pp. 91–103.
14 Y.-S. Wang, Y. Alrefaei and J.-G. Dai, *Front. Mater.*, 2019, **6**, 1–17.
15 A. Katsik, *Adv. Appl. Ceram.*, 2019, 1–13.
16 H. K. Tchakouté, C. H. Rüscher, E. Kamseu, J. N. Y. Djobo and C. Leonelli, *Mater. Chem. Phys.*, 2017, **199**, 280–288.
17 S. Louati, S. Baklouti and B. Samet, *Appl. Clay Sci.*, 2016, **132–133**, 571–578.
18 Y.-S. Wang, J.-G. Dai, Z. Ding and W.-T. Xu, *Mater. Lett.*, 2017, **190**, 209–212.
19 J. N. Y. Djobo, D. Stephan and A. Elimbi, *Eng. Contract.*, 2020, **31**, 101427.
20 M. Mahyar and S. T. Erdogan, *Cem. Concr. Compos.*, 2015, **63**, 96–103.
21 T. Dong, S. Xie, J. Wang, Z. Chen and Q. Liu, *J. Aust. Ceram. Soc.*, 2020, **56**, 175–184.
22 H. Celerier, J. Jouin, N. Tessier-Doyen and S. Rossignol, *J. Non-Cryst. Solids*, 2018, **500**, 493–501.
23 A. Katsiki, T. Hertel, T. Tysmans, Y. Pontikes and H. Rahier, *Materials*, 2019, **12**, 1–15.
24 M. Zribi, B. Samet and S. Baklouti, *J. Non-Cryst. Solids*, 2019, **511**, 62–67.
25 H. Lin, H. Liu, Y. Li and X. Kong, *Cem. Concr. Res.*, 2021, **144**, 106425.
26 J. N. Djobo Yankwa and R. Y. Nkwaju, *RSC Adv.*, 2021, **11**, 32258–32268.
27 Y.-S. Wang, J. L. Provis and J. G. Dai, *Cem. Concr. Compos.*, 2018, **93**, 186–195.
28 J. N. Y. Djobo and D. Stephan, *Cem. Concr. Res.*, 2022, **158**, 106840.
29 A. S. Wagh, *Chemically Bonded Phosphate Ceramics Twenty-First Century Materials with Diverse Applications*, Elsevier Science, Amsterdam, 2nd edn., 2016, vol. 24.
30 A. S. Wagh, in *Chemically Bonded Phosphate Ceramics*, 2016, pp. 141–155.
31 B. Missota Priso Dickson, J. Dika Manga, T. E. Pougnong, J. Baenla, L. Ndongo Ebongue and A. Elimbi, *Silicon*, 2022, **14**, 3693–3705.
32 J. N. Y. Djobo and D. Stephan, *J. Aust. Ceram. Soc.*, 2021, 1145–1154.
33 H. K. Tchakouté, C. H. Rüscher, E. Kamseu, F. Andreola and C. Leonelli, *Appl. Clay Sci.*, 2017, **147**, 184–194.
34 C. Nobouassia Bewa, L. Valentini, H. Kouamo Tchakouté, E. Kamseu, J. N. Yankwa Djobo, M. C. Dalconi, E. Garbin and G. Artioli, *Constr. Build. Mater.*, 2022, **320**, 126302.
35 J. N. Y. Djobo and D. Stephan, *J. Am. Ceram. Soc.*, 2022, **105**, 3226–3237.
36 H. Wei, T. Wang, Q. Zhang, Y. Jiang and C. Mo, *J. Chinese Chem. Soc.*, 2020, **67**, 116–124.
37 M. Lassinantti Gualtieri, M. Romagnoli and A. F. Gualtieri, *J. Eur. Ceram. Soc.*, 2015, **35**, 3167–3178.